Mild covalent functionalization of transition metal dichalcogenides with maleimides: a "click" reaction for TMDCs.

Mariano Vera-Hidalgo, Emerson Giovanelli, Cristina Navío and Emilio M. Pérez*

IMDEA Nanociencia, C/Faraday 9, Ciudad Universitaria de Cantoblanco, 28049, Madrid, SPAIN.

E-mail: emilio.perez@imdea.org.

ABSTRACT: The physical properties of ultrathin transition metal dichalcogenides (2D-TMDCs) make them promising candidates as active nanomaterials for catalysis, optoelectronics, and biomedical applications. Chemical modification of TMDCs is expected to be key in modifying/adding new functions that will help make such promise a reality. We present a mild method for the modification of the basal planes of 2H-MoS_2 and WS_2. We exploit the soft nucleophilicity of sulfur to react it with maleimide derivatives, achieving covalent functionalization of 2H-TMDCs under very mild conditions. Extensive characterization proves that the reaction occurs through Michael addition. Our results adapt one of the most popular "click" reactions in polymer chemistry and biochemistry to obtain a powerful tool for the chemical manipulation of TMDCs.

Transition metal dichalcogenides (TMDCs) are one of the most interesting families of lamellar materials that can be exfoliated down to bidimensional sheets of single or very few layers. (2D-TMDCs).[1-5] The (photo)catalytic properties of 2D-TMDCs had been known for decades,[6] but their electronic properties[7-10] have brought them back to the research spotlight.[11-16]

Chemically, each sheet of a TMDC is composed of a layer of transition metal atoms (M, typically Mo or W) sandwiched between two layers of chalcogen atoms (X, typically S, Se or Te), to which they are covalently bound with MX2 stoichiometry. These three-atom thick TMDC sheets are stacked through van der Waals forces to form the bulk material, and can be separated using mechanical[17] or liquid-phase exfoliation (LPE) techniques.[18-20] While the mechanical exfoliation from the bulk[21] and the synthesis of

monolayers (typically through chemical vapor deposition)[22] have dominated the production of individual 2D-TMDCs to study their physical properties and for the prototyping of (opto)electronic devices, LPE is a complementary approach that renders colloidal suspensions of 2D nanomaterials in much larger amounts.[23,24]

The chemical modification of TMDCs with small molecules has been explored to modify their surface properties (i.e. fine-tune colloidal properties, include specific interactions, etc.) and electronic features (i.e. improve absorption, modify band-gap, etc.).[25,26]

The direct decoration with thiols is the most explored approach for the covalent modification of MoS_2.[27] Initially assumed to proceed *via* covalent attachment of the thiols at sulfur vacancies,[28] this interpretation has recently been called into question, and a different mechanism, involving strong physisorption of disulfides formed *in situ* has been proposed instead.[29] The formation of coordination bonds between metal cations and the sulfur atoms of MoS_2 has also been explored.[30,31] Finally, the nucleophilicity provided by the negative charges left over in the 1T-MoS_2 obtained after chemical exfoliation with n-BuLi has been exploited for functionalization with electrophiles, typically alkyl halides,[32] but also with aryldiazonium salts.[33]

On the other hand, maleimides are the prototypical electrophiles for sulfur-based nucleophiles, reacting through Michael addition, typically under mild conditions and orthogonally to most other functional groups. The robustness of this chemistry has been tried and tested in the biochemistry and polymer chemistry realms, where it has become part of the "click" chemistry toolbox.[34-37]

Here, we exploit the inherent soft nucleophilic character of S to functionalize 2H-MoS_2 and WS_2 covalently with maleimide derivatives at room temperature. As a proof-of-concept application, we have explored the covalent connection of MoS_2 flakes with controlled spacing, using a bis-maleimide reagent.

Few-layer colloids of MoS_2 and WS_2 were obtained by LPE in 2-propanol/water using an ultrasonic probe (7:3 v/v and 1h for MoS_2; 1:1 v/v and 8h for WS_2). This relatively mild exfoliation procedure yields colloids of the 2H polytype TMDCs, as evidenced by UV-vis extinction and Raman

spectroscopies, and high-resolution transmission electron microscopy (HR-TEM, see below), with a majority of flakes in the few layers limit (<10 nm from AFM data), lateral sizes in the hundreds of nm (100-600 nm from TEM data, see the Supporting Information for full characterization). After this process, the solvent of the dispersion was changed to acetronitrile,[38] and *N*-benzylmaleimide and triethylamine were added. The reaction was stirred overnight. Then, the product was centrifuged and washed with acetonitrile several times in order to eliminate excess reagents (see the Supporting Information for experimental details).

The product shows a functionalization of 24% for the maleimide-functionalized MoS_2 flakes (**mal-MoS_2**) and 11% for **mal-WS_2**, estimated from thermogravimetric analysis (Figure 1b). This high degree of functionalization is incompatible with reaction at the edges/defect sites only, and indicates that the basal planes also undergo significant chemical modification.[31,32] The Raman spectra (l_{exc} = 532 nm) of both the pristine and functionalized samples are dominated by the characteristic E^1_{2g} and A_{1g} modes which appear only slightly shifted after functionalization (see the Supporting Information). Comparison of the ATR-IR spectra of the maleimide reagent **mal-MoS_2** and **mal-WS_2** is conclusive with respect to the mode of functionalization. Figure 1c shows the presence of most vibrations of maleimide in both the **mal-MoS_2** and **mal-WS_2** samples, although significantly weaker in the latter case due to the lower degree of functionalization. For instance, the intense carbonyl stretch appears at 1695 cm^{-1} in N-benzylmaleimide and at 1694 cm^{-1} in **mal-MoS_2**, while the aromatic C-H bending are visible at 691 and 723 cm^{-1} and at 691 and 728 cm^{-1} in the reagent and product, respectively. Remarkably, the strong alkene C-H bending mode, clearly visible at 840 cm^{-1} in the spectrum of *N*-benzylmaleimide, is completely depleted in both **mal-MoS_2** and **mal-WS_2**. These observations not only prove that the **mal-MoS_2** and **mal-WS_2** samples are functionalized through a Michael addition mechanism, but also that they contain negligible amounts of physisorbed unreacted N-benzylmaleimide.

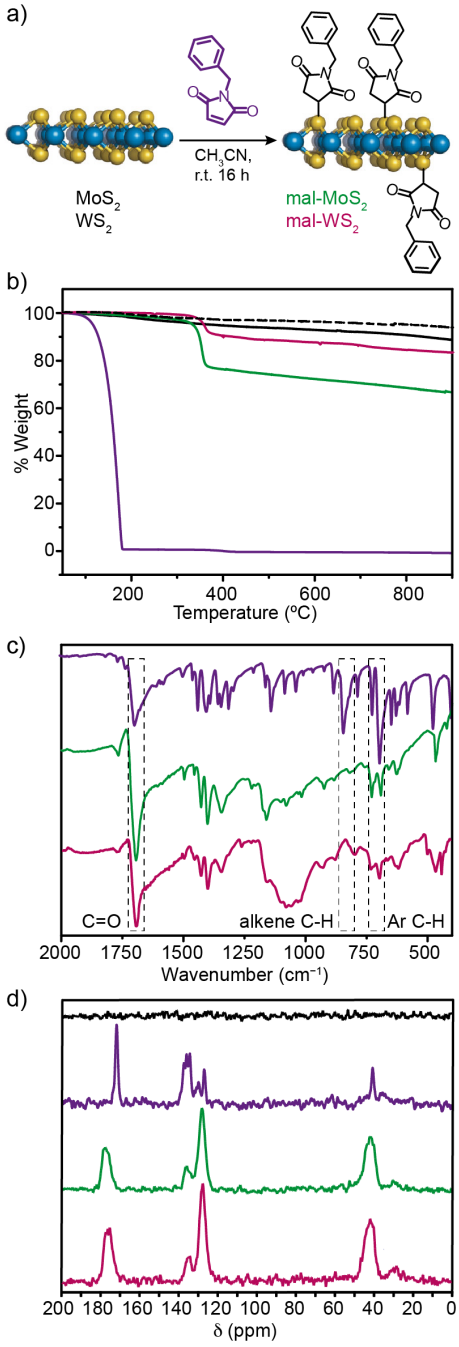

Figure 1. a) General scheme for the functionalization of TMDCs with *N*-benzylmaleimide. b) TGA (N2, 10 ºC min-1) of exfoliated MoS2 (black solid line) and WS2 (black dashed line), **mal-MoS_2** (green), **mal-WS_2** (magenta), and maleimide (purple). The color code is identical for c) and d). c) Comparison of the ATR-IR spectra of maleimide, **mal-MoS_2** and **mal-WS_2**. d) Comparison of the CP-MAS-13C-NMR spectra of MoS2, maleimide, **mal-MoS_2** and **mal-WS_2**.

Solid-state CP-MAS-^{13}C-NMR spectra are shown in Figure 1d. As expected, we observe no signal from the unreacted exfoliated samples. In the *N*-benzylmaleimide spectrum, we observe a relatively weak and sharp signal in the alkyl region, at 40.7 ppm, that can be unambiguously assigned to the methylene group. In the sp^2 region, we find signals between 137.o and 125.0 ppm, which correspond to the phenyl and alkene signals, and the carbonyl group at 171.7 ppm. The evidence for covalent functionalization via Michael addition is unmistakable in the spectra of **mal-MoS_2** and **mal-WS_2**. Although with our set up the CP-MAS-^{13}C-NMR is not quantitative, it is qualitatively obvious that the alkyl signals increase in relative integration and show more than one chemical environment. In parallel with the increase in alkyl signals, in the aromatic-alkene region, the most de-shielded signal, corresponding to the electron-poor alkene, disappears. Finally, the carbonyl signal is significantly shifted downfield, to 177.5 ppm, in agreement with attack by a sulfur nucleophile and saturation of the double bond.

Considering that each sulfur atom in MoS_2 is covalently bound to three Mo/W atoms, the formation of a covalent bond with the maleimide would imply the formation of a hypervalent S species with covalent bonds to three Mo/W atoms and one C atom. Such species have already been documented in the literature of soluble Mo and W clusters.[39-41] Alternatively, the reactivity might arise from S^- present in the structure, due to Mo vacancies created during the LPE or solvent-transfer processes.[42] To explore these hypotheses, we carried out X-ray photoemission spectroscopy (XPS) measurements. The core level of C 1s centered in 284.6 eV was used as a binding energy reference. The main results for MoS_2 are described in Figure 2, depicting the XPS core levels corresponding to the S 2p (left column), Mo 3d and S2s (middle column), and N 1s and Mo $3p_{3/2}$ regions, with their corresponding fits. The process to change solvent from 2-propanol/water (Figure 2a-c) to CH_3CN (Figure 2d-f) already produces observable changes. Although the sharp doublet structures are maintained, the best fit requires including a second component (in gray). However, the changes upon chemical functionalization (Figure 2g-i) are much more obvious. To begin with, the appearance of a clear peak for N 1s (Figure 2i), which can be unambiguously assigned to the maleimide fragment thanks to the comparison with the small shoulder due to residual CH_3CN in the unreacted material (Figure 2f). Furthermore, the S peak becomes

significantly broader and requires a large lower energy contribution at 161.8 eV (green in Figure 2g). Likewise, the Mo signal is best fitted with a new component at 228.6 eV (green in Figure 2h). These changes are consistent with the dominant mechanism for the reaction being the formation of hypervalent S, as proposed above, where the formal negative charge on the S atoms would facilitate extraction of the electrons.

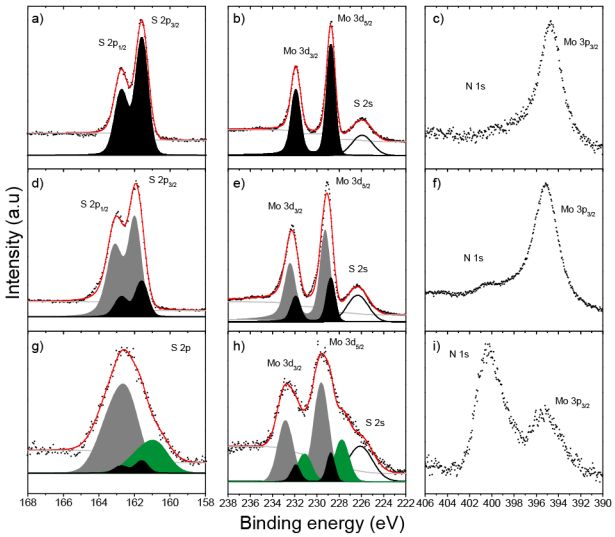

Figure 2. XPS spectra of S, Mo and N core levels for a-c) MoS_2 as obtained in 2-propanol/water. d-f) MoS2 after transfer to CH3CN. g-i) **mal-MoS2.**

Chemical exfoliation/functionalization of TMDCs under harsh conditions typically results in transformation of the semiconducting 2H to the metallic 1T polytype.[26] UV-vis and Raman spectroscopies, as well as HR-TEM show that the semiconducting 2H nature of the TMDCs nanosheets is not altered during our functionalization protocol. Figure 3 shows HR-TEM images of MoS_2 and WS_2 and the corresponding **mal-MoS_2** and **mal-WS_2** samples, where the conservation of the 2H polytype is evidenced by the hexagonal pattern in the 2D fast Fourier transforms (2D FFT, insets in Figure 3).

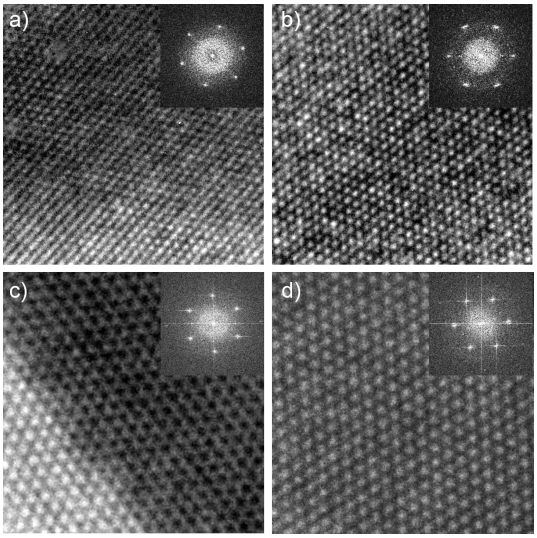

Figure 3. HR-TEM micrographs of a) MoS_2, b) **mal-MoS_2**, c) WS_2 and d) **mal-WS_2**. The insets show the corresponding 2D-fast Fourier transforms.

An interesting macroscopic consequence of the chemical functionalization with organic fragments is that it brings about a noticeable increase of the stability of the colloids in organic solvents, like $CHCl_3$. The increase in colloidal stability in nonpolar solvents is accompanied with a decrease – in absolute value – in the zeta potential (z = −48 mV for MoS_2 and −39 mV for **mal-MoS_2**; −45 mV for WS_2 and −39 mV for **mal-WS_2**) indicating that the improvement in solubility arises from a more oleophilic character of the **mal-MoS2** and **mal-WS2** surface, compared to the starting materials (see the Supporting Information).

The vertical connection of different 2D materials, typically by manually stacking one material on top of the other[43] has given rise to the emerging field of van der Waals heterostructures.[44] An interesting and much less explored alternative to generate novel nanomaterials with enhanced properties is their covalent cross-linking.[45-47] In the case of single-layer MoS2, for instance, one could envisage connecting several nanosheets through suitable molecular spacers to conserve the direct bandgap of single layer MoS_2 while effectively multiplying its light absorption/emission properties.[48]

With the maleamide-TMDC chemistry clearly established, we decided to try to build covalently-linked vertical MoS_2-MoS_2 homostructures as a proof-of-concept application. To that end, we reacted a

commercially available bismaleimide reagent (chemical structure in Figure 4a) with MoS_2 colloidal suspensions, following the protocols described above. The product isolated from such reaction (**MoS2-mal-mal-MoS2** in Figure 4a) shows a significant increase in the scattering contribution to the extinction UV-vis spectrum compared to both MoS2 and **mal-MoS2**. Moreover, in contrast with **mal-MoS2**, its colloidal stability in $CHCl_3$ decreases significantly compared to the parent MoS2, and even more so compared to **mal-MoS2**, most likely due to a combination of the increase in particle size observed in the extinction spectrum and the organic addend being not so exposed to the solvent (see the Supporting Information). AFM analyses of dropcasts of **MoS2**, and **MoS2-mal-mal-MoS2** shed light on this matter (Figure 4b-d). While there is no signifiant change in either the height or area of the nanosheets upon MoS2 to **mal-MoS2** functionalization (see the Supporting Information), the flakes of **MoS2-mal-mal-MoS2** show a substantial increase in thickness and, to a lesser extent, area (Figure 4d). Since the starting MoS2 suspension is identical for both reactions, such changes can be directly attributed, respectively, to basal plane-to-basal plane vertical connection and edge-to-edge horizontal connection of MoS2 nanosheets through **mal-mal** linkers. Indeed, under TEM microscopy we observe at several instances few-layer MoS_2 flakes (distance between layers ca. 0.6 nm) connected by ca. 1-0.8 nm spacing. The TEM data corresponds reasonably well to the estimated distance between two small fragments of MoS_2 separated by the mal-mal spacer (1.2 nm, molecular mechanics, see the Supporting Information).[49]

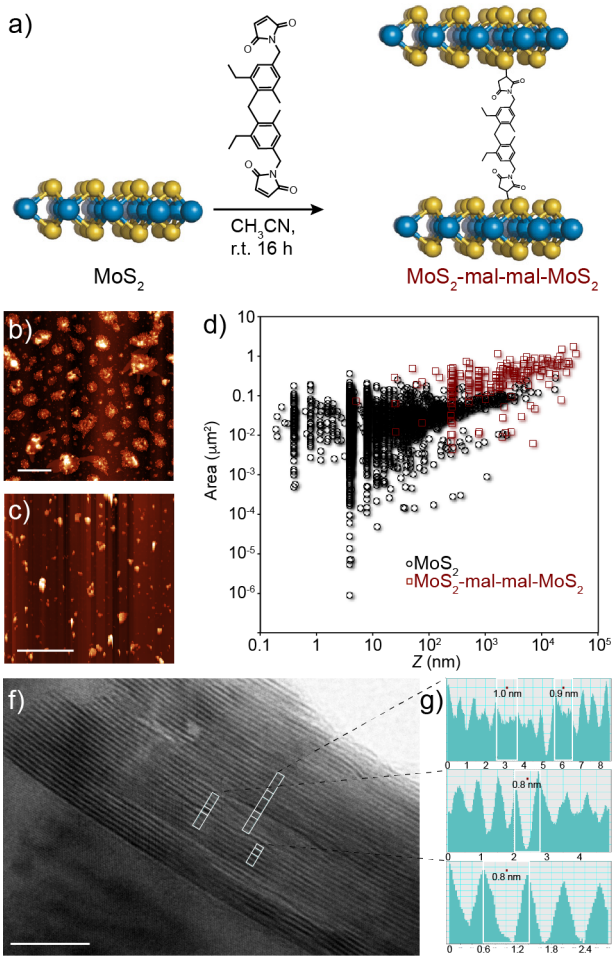

Figure 4. a) General scheme for the covalent cross-linking of MoS2 with a bismaleimide reagent, depicted as an idealized vertical connection. Representative AFM topography micrographs of b) MoS2, scale bar is 1 mm and c) **MoS2-mal-mal-MoS2**, scale bar is 10 mm d) Scatter plot of areaarea vs height (median) data as obtained from the micrographs shown in b) and c). f) TEM image of the edge region of a multilayer MoS2-mal-mal-MoS2 flake, scale bar is 10 nm. g) Contrast profiles obtained from the regions marked in white in f).

In summary, we develop a new strategy for the covalent functionalization of TMDCs, based on the avidity of S as a soft nucleophile for soft electrophiles. In particular, we describe that 2H-MoS2 and WS2 can be covalently functionalized with maleimide reagents via Michael addition. The reaction occurs at room temperature, under very mild conditions that do not affect the electronic structure of the TMDCs.

Our results will allow those interested in the chemistry of TMDCs to tap into the rich toolbox of maleimide-based reagents developed to modify proteins and polymers, many even commercially available, or design "a la carte" reagents using well-established chemistry on the maleimide.

ASSOCIATED CONTENT

Supporting Information. Supplementary figures and detailed experimental procedures.

AUTHOR INFORMATION

Corresponding Author

*emilio.perez@imdea.org

ACKNOWLEDGMENT

Funding from the European Union (ERC-StG-307609), MINECO (CTQ2014-60541-P and CTQ2017-86060-P) the Comunidad de Madrid (MAD2D-CM S2013/MIT-3007) is gratefully acknowledged. IMDEA Nanociencia acknowledges support from the "Severo Ochoa" Programme for Centres of Excellence in R&D (MINECO, Grant SEV-2016-0686). We thank the National Centre for Electron Microscopy (ICTS-CNME, Universidad Complutense) for electron microscopy facilities.

REFERENCES

(1) Hu, Z.; Wu, Z.; Han, C.; He, J.; Ni, Z.; Chen, W. *Chem. Soc. Rev.* **2018**, *47*, 3100.

(2) Han, G. H.; Duong, D. L.; Keum, D. H.; Yun, S. J.; Lee, Y. H. *Chem. Rev.* **2018**, *118*, 6297.

(3) Mak, K. F.; Shan, J. *Nat. Photonics* **2016**, *10*, 216.

(4) Jariwala, D.; Sangwan, V. K.; Lauhon, L. J.; Marks, T. J.; Hersam, M. C. *ACS Nano* **2014**, *8*, 1102.

(5) Wang, Q. H.; Kalantar-Zadeh, K.; Kis, A.; Coleman, J. N.; Strano, M. S. *Nat. Nanotechnol.* **2012**, *7*, 699.

(6) Frindt, R. F. *J. Appl. Phys.* **1966**, *37*, 1928.

(7) Radisavljevic, B.; Radenovic, A.; Brivio, J.; Giacometti, V.; Kis, A. *Nat. Nanotechnol.* **2011**, *6*, 147.

(8) Lopez-Sanchez, O.; Lembke, D.; Kayci, M.; Radenovic, A.; Kis, A. *Nat. Nanotechnol.* **2013**, *8*, 497.

(9) Eda, G.; Yamaguchi, H.; Voiry, D.; Fujita, T.; Chen, M.; Chhowalla, M. *Nano Lett.* **2011**, *11*, 5111.

(10) Mak, K. F.; Lee, C.; Hone, J.; Shan, J.; Heinz, T. F. *Phys. Rev. Lett.* **2010**, *105*, 136805.

(11) Castellanos-Gomez, A.; van Leeuwen, R.; Buscema, M.; van der Zant, H. S. J.; Steele, G. A.; Venstra, W. J. *Adv. Mater.* **2013**, *25*, 6719.

(12) Castellanos-Gomez, A.; Roldan, R.; Cappelluti, E.; Buscema, M.; Guinea, F.; van der Zant, H. S. J.; Steele, G. A. *Nano Lett.* **2013**, *13*, 5361.

(13) Kang, K.; Xie, S.; Huang, L.; Han, Y.; Huang, P. Y.; Mak, K. F.; Kim, C.-J.; Muller, D.; Park, J. *Nature* **2015**, *520*, 656.

(14) Yu, Y.; Nam, G.-H.; He, Q.; Wu, X.-J.; Zhang, K.; Yang, Z.; Chen, J.; Ma, Q.; Zhao, M.; Liu, Z.; Ran, F.-R.; Wang, X.; Li, H.; Huang, X.; Li, B.; Xiong, Q.; Zhang, Q.; Liu, Z.; Gu, L.; Du, Y.; Huang, W.; Zhang, H. *Nat. Chem.* **2018**, *10*, 638.

(15) Xie, S.; Tu, L.; Han, Y.; Huang, L.; Kang, K.; Lao, K. U.; Poddar, P.; Park, C.; Muller, D. A.; DiStasio, R. A., Jr.; Park, J. *Science* **2018**, *359*, 1131.

(16) Si, M.; Su, C.-J.; Jiang, C.; Conrad, N. J.; Zhou, H.; Maize, K. D.; Qiu, G.; Wu, C.-T.; Shakouri, A.; Alam, M. A.; Ye, P. D. *Nat. Nanotechnol.* **2018**, *13*, 24.

(17) Li, H.; Wu, J.; Yin, Z.; Zhang, H. *Acc. Chem. Res.* **2014**, *47*, 1067.

(18) Cunningham, G.; Lotya, M.; Cucinotta, C. S.; Sanvito, S.; Bergin, S. D.; Menzel, R.; Shaffer, M. S. P.; Coleman, J. N. *ACS Nano* **2012**, *6*, 3468.

(19) Coleman, J. N.; Lotya, M.; O'Neill, A.; Bergin, S. D.; King, P. J.; Khan, U.; Young, K.; Gaucher, A.; De, S.; Smith, R. J.; Shvets, I. V.; Arora, S. K.; Stanton, G.; Kim, H.-Y.; Lee, K.; Kim, G. T.; Duesberg, G. S.; Hallam, T.; Boland, J. J.; Wang, J. J.; Donegan, J. F.; Grunlan, J. C.; Moriarty, G.; Shmeliov, A.; Nicholls, R. J.; Perkins, J. M.; Grieveson, E. M.; Theuwissen, K.; McComb, D. W.; Nellist, P. D.; Nicolosi, V. *Science* **2011**, *331*, 568.

(20) Bernal, M. M.; Alvarez, L.; Giovanelli, E.; Arnaiz, A.; Ruiz-Gonzalez, L.; Casado, S.; Granados, D.; Pizarro, A. M.; Castellanos-Gomez, A.; Perez, E. M. *2D Mater.* **2016**, *3*, 035014/1.

(21) Castellanos-Gomez, A.; Buscema, M.; Molenaar, R.; Singh, V.; Janssen, L.; van der Zant, H. S. J.; Steele, G. A. *2D Mater.* **2014**, *1*, 011002/1.

(22) Lv, R.; Robinson, J. A.; Schaak, R. E.; Sun, D.; Sun, Y.; Mallouk, T. E.; Terrones, M. *Acc. Chem. Res.* **2015**, *48*, 56.

(23) Smith, R. J.; King, P. J.; Lotya, M.; Wirtz, C.; Khan, U.; De, S.; O'Neill, A.; Duesberg, G. S.; Grunlan, J. C.; Moriarty, G.; Chen, J.; Wang, J.; Minett, A. I.; Nicolosi, V.; Coleman, J. N. *Adv. Mater.* **2011**, *23*, 3944.

(24) Zhang, X.; Lai, Z.; Tan, C.; Zhang, H. *Angew. Chem., Int. Ed.* **2016**, *55*, 8816.

(25) Hirsch, A.; Hauke, F. *Angew. Chem., Int. Ed.* **2017**, *57*, 4338.

(26) Bertolazzi, S.; Gobbi, M.; Zhao, Y.; Backes, C.; Samori, P. *Chem. Soc. Rev.* **2018**, *47*, 6845.

(27) Presolski, S.; Pumera, M. *Materials Today* **2016**, *19*, 140.

(28) Chou, S. S.; De, M.; Kim, J.; Byun, S.; Dykstra, C.; Yu, J.; Huang, J.; Dravid, V. P. *J. Am. Chem. Soc.* **2013**, *135*, 4584.

(29) Chen, X.; Berner Nina, C.; Backes, C.; Duesberg Georg, S.; McDonald Aidan, R. *Angew. Chem., Int. Ed.* **2016**, *55*, 5803.

(30) Liu, Y.-T.; Tan, Z.; Xie, X.-M.; Wang, Z.-F.; Ye, X.-Y. *Chem. Asian J.* **2013**, *8*, 817.

(31) Backes, C.; Berner Nina, C.; Chen, X.; Lafargue, P.; LaPlace, P.; Freeley, M.; Duesberg Georg, S.; Coleman Jonathan, N.; McDonald Aidan, R. *Angew. Chem., Int. Ed.* **2015**, *54*, 2638.

(32) Voiry, D.; Goswami, A.; Kappera, R.; Silva, C. d. C. C. e.; Kaplan, D.; Fujita, T.; Chen, M.; Asefa, T.; Chhowalla, M. *Nature Chem.* **2014**, *7*, 45.

(33) Knirsch, K. C.; Berner, N. C.; Nerl, H. C.; Cucinotta, C. S.; Gholamvand, Z.; McEvoy, N.; Wang, Z.; Abramovic, I.; Vecera, P.; Halik, M.; Sanvito, S.; Duesberg, G. S.; Nicolosi, V.; Hauke, F.; Hirsch, A.; Coleman, J. N.; Backes, C. *ACS Nano* **2015**, *9*, 6018.

(34) Bhatia, S. K.; Shriver-Lake, L. C.; Prior, K. J.; Georger, J. H.; Calvert, J. M.; Bredehorst, R.; Ligler, F. S. *Anal. Biochem.* **1989**, *178*, 408.

(35) Kade, M. J.; Burke, D. J.; Hawker, C. J. *J. Polym. Sci., Part A: Polym. Chem.* **2010**, *48*, 743.

(36) Hoyle, C. E.; Bowman, C. N. *Angew. Chem., Int. Ed.* **2010**, *49*, 1540.

(37) Northrop, B. H.; Frayne, S. H.; Choudhary, U. *Polym. Chem.* **2015**, *6*, 3415.

(38) Giovanelli, E.; Castellanos-Gomez, A.; Perez, E. M. *ChemPlusChem* **2017**, *82*, 732.

(39) Matsumoto, T.; Namiki, R.; Chang, H.-C. *Eur. J. Inorg. Chem.* **2018**, Ahead of Print.

(40) Gomes de Lima, M. B.; Guerchais, J. E.; Mercier, R.; Petillon, F. Y. *Organometallics* **1986**, *5*, 1952.

(41) Ellis, J. E.; Rochfort, G. L. *Organometallics* **1982**, *1*, 682.

(42) Hai, X.; Chang, K.; Pang, H.; Li, M.; Li, P.; Liu, H.; Shi, L.; Ye, J. *J. Am. Chem. Soc.* **2016**, *138*, 14962.

(43) Geim, A. K.; Grigorieva, I. V. *Nature* **2013**, *499*, 419.

(44) Liu, Y.; Weiss, N. O.; Duan, X.; Cheng, H.-C.; Huang, Y.; Duan, X. *Nat. Rev. Mater.* **2016**, *1*, 16042.

(45) Rao, C. N. R.; Pramoda, K.; Kumar, R. *Chem. Commun.* **2017**, *53*, 10093.

(46) Schirowski, M.; Abellan, G.; Nuin, E.; Pampel, J.; Dolle, C.; Wedler, V.; Fellinger, T.-P.; Spiecker, E.; Hauke, F.; Hirsch, A. *J. Am. Chem. Soc.* **2018**, *140*, 3352.

(47) Bernal, M. M.; Di Pierro, A.; Novara, C.; Giorgis, F.; Mortazavi, B.; Saracco, G.; Fina, A. *Adv. Funct. Mater.* **2018**, *28*, n/a.

(48) Zhao, W.; Ribeiro, R. M.; Eda, G. *Acc. Chem. Res.* **2015**, *48*, 91.

(49) The calculated distance is best understood as an upper limit for experimental observation. To measure exactly 1.25 nm would require that the flakes were heavily functionalized at the site of observation. In all other cases, the MoS2 flakes will tend to reduce this distance, maximizing van der Waals interactions.

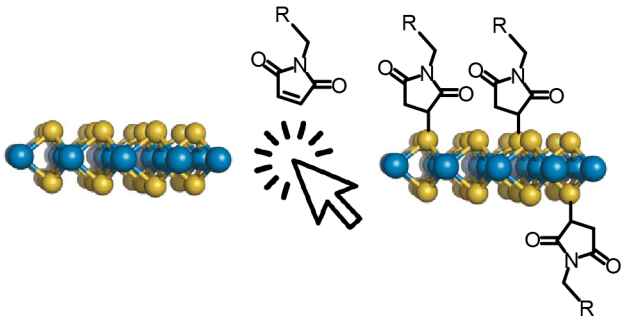
R
O
N
O
R
O
N
O
R
O
N
O
O
N
O
R